# Supporting Information

## Table-top Combined Scanning X-ray Small Angle Scattering and Transmission Microscopies of Lipid Vesicles dispersed in free-standing Gel

F. Scattarella[1], E. Altamura[2], P. Albanese[2], D. Siliqi[1], M. Ladisa[1,§], F. Mavelli[2], C. Giannini[1] and D. Altamura[1,*]

[1]Istituto di Cristallografia - CNR, Via Amendola 122/O, 70126 Bari, Italy

[2]Chemistry Department University of Bari Aldo Moro, via Orabona 4, 70125 Bari, Italy

[§]Present address : Istituto per le Applicazioni del Calcolo "Mauro Picone"-CNR, Via Amendola 122/O, 70126 Bari, Italy

*Corresponding author: davide.altamura@ic.cnr.it

### *A. Normalization of the SAXS intensity to sample absorption and thickness*

Due to sample absorption, the measured SAXS intensity ($I_{SAXS}$) is only a fraction T of the actual scattered intensity ($I_0$). Assuming that the fraction of photons scattered by the sample is negligible compared to unscattered (transmitted) ones, T can be approximated as the ratio between the intensities of the unscattered and primary beams. The last are measured by a pin diode in the beamstop, when the X-ray beam is passing or not through the sample, respectively. Based on the Lambert-Beer law (ref. [38] of the main text), $I_{SAXS} = I_0 * e^{-\mu t} = I_0 * T$ , where $\mu$ is the absorption coefficient of the sample.

In the case of constant film thickness ($t$), the $T$ maps directly provide the lateral variation of the X-ray absorption coefficient (i.e. of the local material density); the $I_{SAXS}/T$ maps provide therefore a correction of the scattered intensity according to the local $\mu$ variations, specifically highlighting the scattering contrast. Moreover, information on the average film density and thickness can in turn be obtained and compared between different samples, as shown in [1].

In the general case of samples with uneven thickness, $T$ maps represent the overall variations of the $\mu * t$ product. By expressing sample thickness values as multiples of a reference thickness value ($t_0$) as $t = n * t_0$, in the case of approximately constant $\mu$, the transmission coefficient ($T$) will have a power law dependence on $n$ (i.e. $T \sim T_0^n$), as derived by directly substituting the expression for $t$ in the Lambert-Beer law (being $T_0$ the transmission coefficient corresponding to the reference thickness $t_0$). Hence, once $t_0$ is chosen (it must be the same for both GEL and POPC samples):

$$I_{SAXS(reference)} = I_{0(reference)} e^{-\mu t_0} = I_{0(reference)} T_{(reference)}$$

$$I_{SAXS(sample)} = I_{0(sample)} e^{-\mu n t_0} = I_{0(sample)} T_{(sample)} = I_{0(sample)} T^n_{(reference)}$$

where $I_{0(sample)}$ *and* $I_{0(reference)}$ could differ from each other due to fluctuations of the X-ray source.

Being $T_{(sample)} = \frac{I_{SAXS(sample)}}{I_{0(sample)}}$ , the relative thickness $n$ is then readily derived:

$$T_{(sample)} = T^{n}_{(reference)}$$

$$n = \frac{\ln\left(T_{(sample)}\right)}{\ln\left(T_{(reference)}\right)}$$

It is worth to note that the scatterer (lipids in our case) absorption contribution is here neglected, so that this formulation accounts for diluted/non-absorbing objects dispersed in an absorbing matrix with arbitrary volume and shape, although it can be generalized to the case of absorbing scatterers.

Since the scattered intensity from different sample areas with similar structural features (and similar concentration of scatterers) is proportional to the illuminated sample volume, for a given beam footprint on the sample the scattered intensity will be proportional to sample thickness, hence to *n.*

Therefore: plotting the scattered intensity normalized to the T coefficient ($I_{SAXS}/T$) leads to a spatial map of the actual SAXS intensity; the further normalization to *n* ($I_{SAXS}/T/n$) provides the relative SAXS intensity distribution, i.e. changes in scatterer concentration are probed. Since the microscopies are 2D projections (i.e. the SAXS contribution is integrated along the beam propagation direction), they provide a quantitative average across sample thickness.

All 1D folded SAXS patterns analysed in this work can be thus quantitatively compared, all being related to the same sample reference volume.

*B. SAXS 1D folding and averaging*

The 1D folded SAXS profiles averaged over the high and low concentration ROIs highlighted in Figs. 1h and 2h are reported in Figs. S2 and S7, respectively, both before and after buffer (GEL profile) subtraction. Approximately the same ROIs were considered in the comparison between the wet and dry POPC sample. The very same POPC sample was studied in both conditions consecutively, without being removed; whereas in the case of the bare gel, two different replicas were analyzed at room and low pressure, respectively, and ROIs with different density/scattering features were chosen for comparison, based on similar criteria as for the POPC sample.

In Fig. S1, SAXS profiles from the reduced ($I_{SAXS}/T/n$) maps are reported without and with (Fig. S1 a and b, respectively) subtraction of a “buffer” profile, to show the different intensity scale and slope in different GEL regions (Fig. S1a), and between the resulting difference SAXS profiles in GEL and POPC samples (Fig. S1b). Based on both the higher intensity and slope at low Q values in the relevant SAXS curve (black line in Fig. S1a), the bright spot is ascribed to an aggregate from agar or an impurity. The former option is supported by the plots in Fig. S1b, where a single SAXS profile (from the homogeneous central region ROI 3) has been subtracted as a “buffer” to the same aggregate profile in Fig. S1a, and the result (yellow line) is compared to the SAXS difference profile from GEL regions (ROIs 2 and 1) without aggregates, to show the structure similarity of gel aggregates compared to diluted regions (yellow and green lines respectively). The green line (difference profile between GEL areas) has been also reproduced with green circles and rescaled to show the full overlap to the yellow line (aggregate). Moreover, in Fig. S1b the SAXS difference profiles from high scattering single points in the POPC sample (ROIs 1 and 2, where single profiles from GEL regions ROIs 1 and 2 were used as “buffer”, respectively) are also compared to the profile of the GEL aggregate, to show the significantly different slope at low Q values, and hence the low degree of lipid aggregation. In the

following Fig. S2b, the scattering contribution from aggregated and non-aggregated lipids is compared, to show how the aggregate contribution is negligible in the areal average.

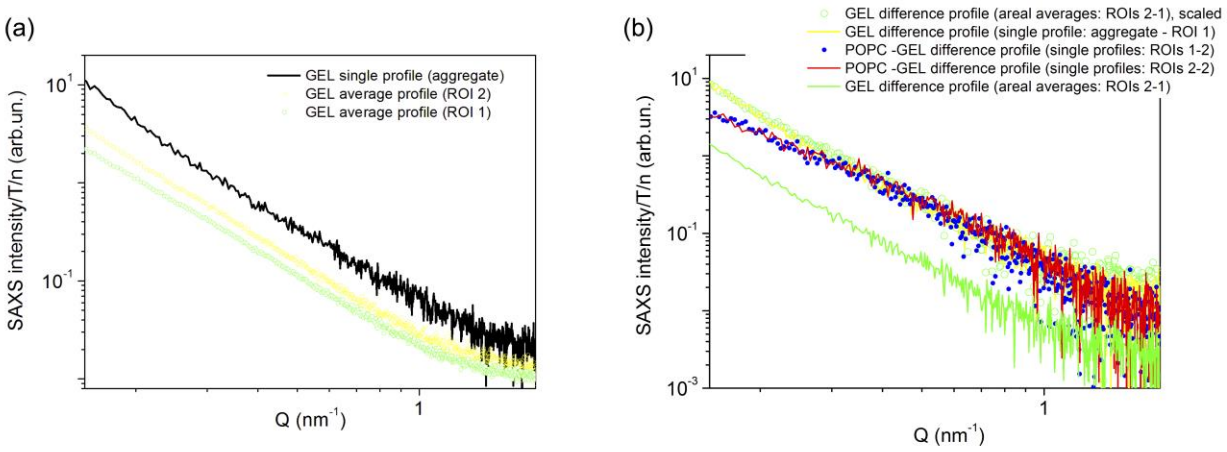


**Fig. S1.** a) The normalized SAXS profiles relevant to the bright point (black line) and arbitrary points in the central (ROI 1) and peripheral (ROI 2) regions in the GEL microscopy (Fig. 1d) are compared, to show the significant intensity difference as well as a difference in the slope in the low Q region (the colour code corresponds to Fig. 1d). b) Normalized SAXS difference profiles from high scattering single points indicating aggregates both in the gel and POPC (ROIs 1 and 2) samples, highlighting the significant slope difference in the low Q region between gel and lipid aggregates. The difference profile from the aggregate in the bare gel is also compared to the difference profile averaged over a central region in the GEL sample to show the structural similarity (single and average SAXS profiles from ROI 1 are used as buffer profiles, respectively). The green circles represent the green line reproduced with an arbitrary scale factor to show the full overlap with the yellow line.

In Fig. S2a, the average unsubtracted SAXS profiles from ROIs 2 of the POPC and GEL samples are reported, showing the three considered Q-ranges corresponding respectively to the smaller and larger intensity difference between the two curves ($\Delta Q_{Gel}$), as well as the ranges dominated by the bilayer Form factor ($\Delta Q_{Form}$), or by correlation effects leading to Bragg diffraction ($\Delta Q_{Bragg}$). In Fig. S2b, the areal averaged SAXS profiles from ROIs 1, 2 and 3 of the POPC sample shown in Fig. 1h, upon buffer subtraction, are reported and compared with the profiles relevant to the lipid aggregates reproduced from Fig. S1b, showing how the different SAXS slope allows to discriminate the local presence of aggregates, although their contribution in the areal average is negligible. This is confirmed by the similarity between the average SAXS profile (magenta line) from the no-aggregates region (ROI 3), and those featuring aggregates (ROIs 1 and 2, blue and red lines), basically differing only by the intensity scale and SNR due to different POPC concentration. It is worth to note that no appreciable difference profile could be obtained from single points in the low scattering central region (ROI 3 in Fig. 1h), whereas it could be obtained as an areal average.

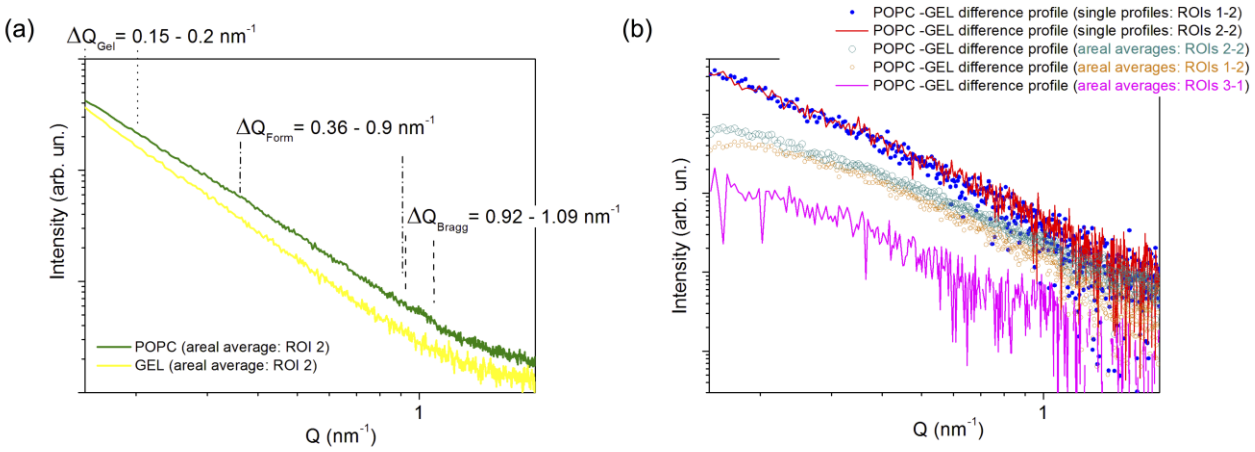


**Fig. S2.** (a) 1D folded SAXS intensity profiles averaged over the ROIs 2 in Fig. 1d,h (main text) are shown as an example: the considered Q-ranges are also shown, relevant to small (0.15÷0.20 $nm^{-1}$) or large contribution of the vesicle/bilayer form factor (0.36÷0.90 $nm^{-1}$), and Bragg diffraction (0.92÷1.09 $nm^{-1}$) from interacting bilayers, respectively, in the wet samples; (b) SAXS difference profiles (reproduced from Fig. S1b) from the high scattering single points (red line and blue dots), and from the areal average over ROIs 1 (orange circles), 2 (dark cyan symbols) and 3 (magenta line) shown in the microscopy of Fig. 1h (main text, with the same colour code), showing the different SAXS intensities relevant to high and low POPC concentration, as well as between aggregates and vesicles. No appreciable difference profile could be obtained from single points in the low scattering central region (ROI 3 in Fig. 1h), whereas it could be obtained as an areal average (magenta line).

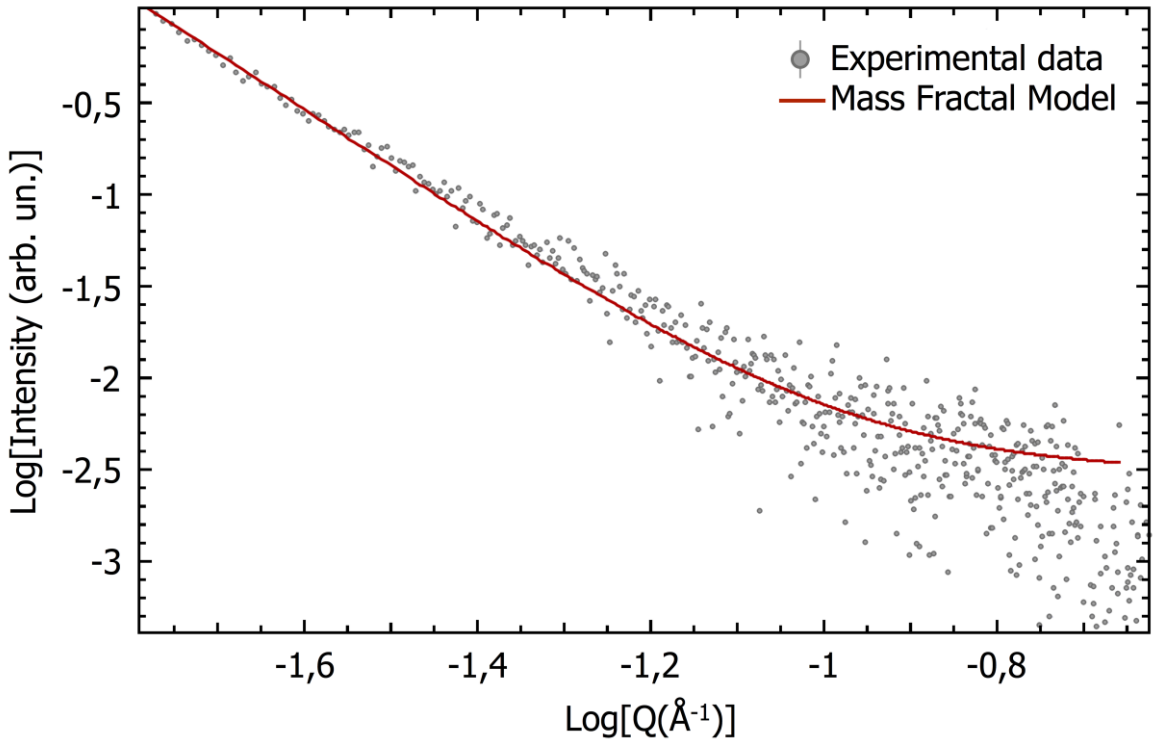


**Fig. S3.** Fit of the SAXS difference profile (Log-Log scale) from ROIs 1 and 2 of the GEL sample, reported in Fig. S1b (green curve). A mass fractal model ([2] in the program SasView) is used, returning a fractal dimension of 2.78.

C. *SAXS profile analysis*

SAXS profiles from the wet POPC sample were fitted, based on the shape-independent or shape-dependent models, respectively, and reported below.

Shape-independent SAXS model

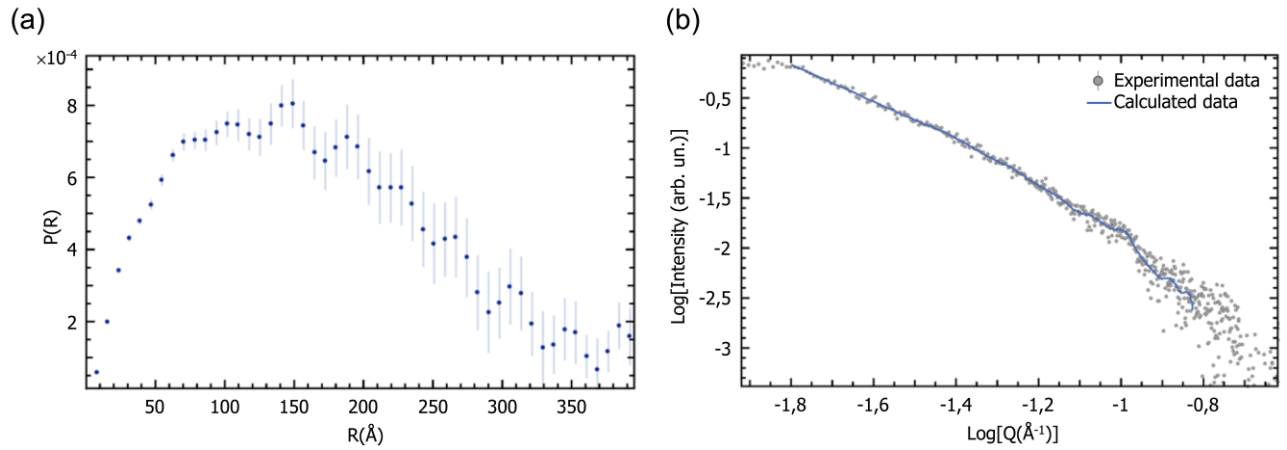


**Fig. S4.** (a): Pair distance distribution, P(R). (b): calculated data from P(R) function and fitted to the SAXS experimental data (Log-Log scale): the power-law decay with exponent equal to -2 ($I(Q)\sim Q^{-2}$) is compatible with a disc-shaped object.

Shape-dependent SAXS model (Multilayer Vesicle [3])

All parameters were let free to vary, according to the consolidated procedure for the cases of multiparametric systems, refining by grouping the parameters, first without the use of polydispersity, and only at the end by adding it.

The 1D scattering intensity *P(Q)* is calculated in the following way [4]

$$P(Q) = scale \cdot \frac{\varphi}{V(R_N)} F^2(Q) + background$$

where

$$F(Q) = (\rho_{shell} - \rho_{solv}) \sum_{i=1}^{N} \left[ 3V(r_i) \frac{\sin(Qr_i) - Qr_i \cos(Qr_i)}{(Qr_i)^3} - 3V(R_i) \frac{\sin(QR_i) - QR_i \cos(QR_i)}{(QR_i)^3} \right]$$

for

$$r_i = r_c + (i-1)(t_s + t_w) \text{ solvent radius before shell } i$$
$$R_i = r_i + t_s \text{ shell radius for shell } i$$

$\varphi$ is the volume fraction of particles, *V(r)* is the volume of a sphere of radius *r*, $r_c$ is the radius of the core, $t_s$ is the thickness of the shell, $t_w$ is the thickness of the solvent layer between the shells, $\rho_{shell}$ is the scattering length density of a shell, and $\rho_{solv}$ is the scattering length density of the solvent.

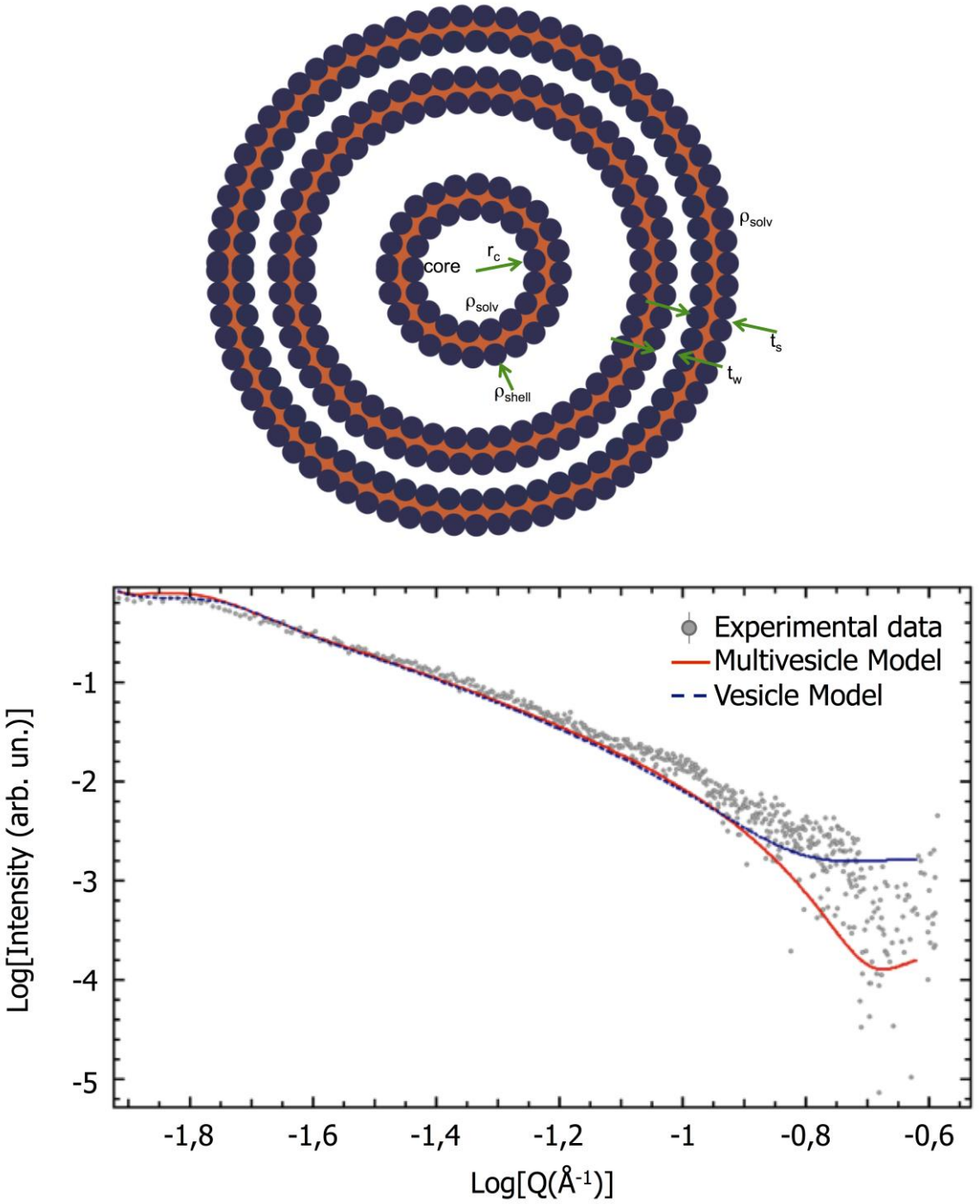


**Fig. S5.** Top: Scheme of the geometrical parameters of the spherical vesicle. Bottom: fit of the SAXS data with multilamellar (solid line) and unilamellar (dashed line) vesicle models (Log-Log scale). The weak Bragg peak around 0.1 Å$^{-1}$ is not considered in the models.

*D. Enhancement of T and n contrast in dry samples*

In the case of dry samples, the weak absorption contribution from lipids, as well as of the solid moiety in the gel, can now be revealed (no more absorption by water), but instrumental background variations due to drifts of the primary beam intensity measured by the pin diode disperses the absorption contrast from

lipids. The no-sample regions in Figs. 1a,e and Fig. S6a show indeed that the precision for the measured transmission coefficient in the sample (including possible inhomogeneities of the medium, e.g. the ultralene sachet) is within ± 5% in the best case, but can be twice this value in the worst case, becoming comparable to the T gradients observed in the dry samples. As a consequence, the as collected T maps (and their correspondent *n* maps) of the dried samples (Fig. S6a,b) are no more representative of the actual density/thickness distribution in the sample, being this merged with background fluctuations, whereby only the overall sample shape is recognized in Fig. S6a,b. Consequently, the normalized SAXS map is also dominated by T fluctuations (Fig. S6c).

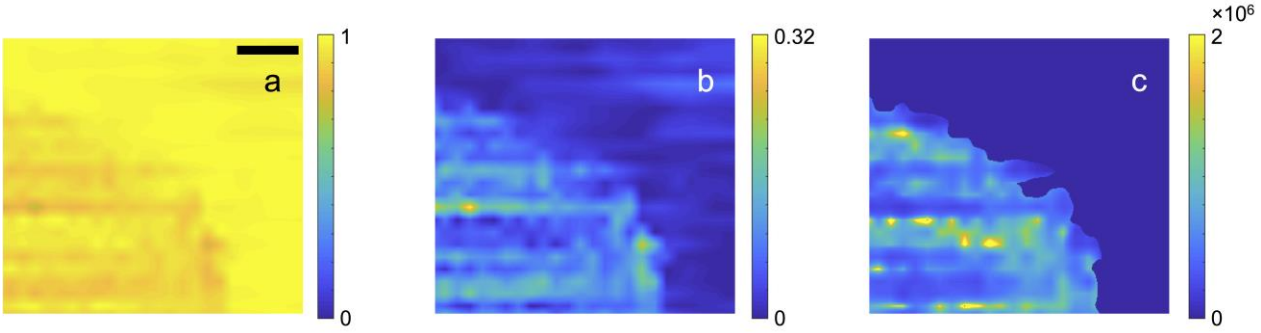


**Fig. S6.** (a) Transmissivity ($T_{row}$) and (b) relative thickness (*n*) maps of dried gels containing POPC lipids, obtained without background compensation and filtering, showing no representative sample features (compare with Fig. 2e,f,h, respectively, in the main text); (c) normalized SAXS microscopy to T and *n*, showing the complete loss of scattering features, compared to the as-collected microscopy in Fig. 2g.

Contrast improvement is achieved in this case by evaluating the background intensity at the border of the transmitted intensity map ($I_{trans}$, not shown), i.e. in the no-sample area, then applying a row by row correction to compensate either irregularities or intensity spikes in the background, over the whole area of the microscopy. Subsequently, the intensity of the background is evaluated row-by-row from the intensity value at the border of the so-correct $I_{trans}$ map, and was used to calculate the new transmission map $T_{row}$. Finally, a Gaussian kernel of 5x5 pixels (4% of the size of the raw $I_{trans}$ map) with a standard deviation of 0.7 has been convolved with $T_{row}$. This method allowed to transform a spot-like T map, dominated by background spikes, in a $T_{row}$ map representative of sample absorption, bringing out local gradients of the transmission coefficient in the sample having mean variation smaller than 10%, thus comparable with background fluctuations.

E. *Masking no-sample regions*

In order to optimize the display of the normalized SAXS maps, and clearly highlight the sample region, a masking procedure was applied to the no-sample area. The reason for this procedure is linked to secondary effects due to the normalization of the SAXS map to *n*, in particular occurring where *n* has values close or equal to zero (i.e. close to sample borders and outside the sample), leading to indeterminate values of the SAXS/*n* ratio. These points would saturate the final colour map and would make the features of the sample almost invisible. To overcome this drawback, a segmentation procedure based on the Region Growing algorithm (ref. [41] in the main text) was applied, which allows creating a binary mask in the normalized

SAXS map resulting in a well-defined sample area. The Region Growing algorithm is based on the examination of the pixels close to an initial point (seed), taken in our case in the background area as the point of minimum relative thickness $n_{min}$ of the entire map, and on the subsequent iterative determination whether the neighbouring pixel should be added or not to the region, based on a similarity criterion. In this way, the normalized SAXS maps shown in Figs. 1 and 2 were created by applying different thresholds of similarity for the different maps.

*F: SAXS & XRD of dry samples*

Only a clear diffraction ring, corresponding to a d-spacing of 5.6±0.1 nm, is clearly visible in vacuum (black line in Fig. S8), also due to the limited accessible Q-range. Such a ring proves the presence of (stacks of) POPC bilayers, as confirmed by the XRD pattern obtained from dried bilayers directly deposited on a silicon wafer and reported in Fig. S8 (blue line), where the two measurements have been rescaled for convenience. Several sharp equally spaced peaks result from the dry lipids on flat substrate, indicating main lamellar stacks of several well-ordered lipid bilayers with a periodicity of 5.9±0.1 nm (calculated as $2\pi/\Delta Q$ from the $\Delta Q$ spacing between high order peaks). Further minor contributions corresponding to slightly different periodicities are recognized as well (Fig. S8): in particular, a quite smaller one (4.9±0.1 nm) from a minority population (only two weak diffraction orders can be glimpsed, as indicated by asterisks).

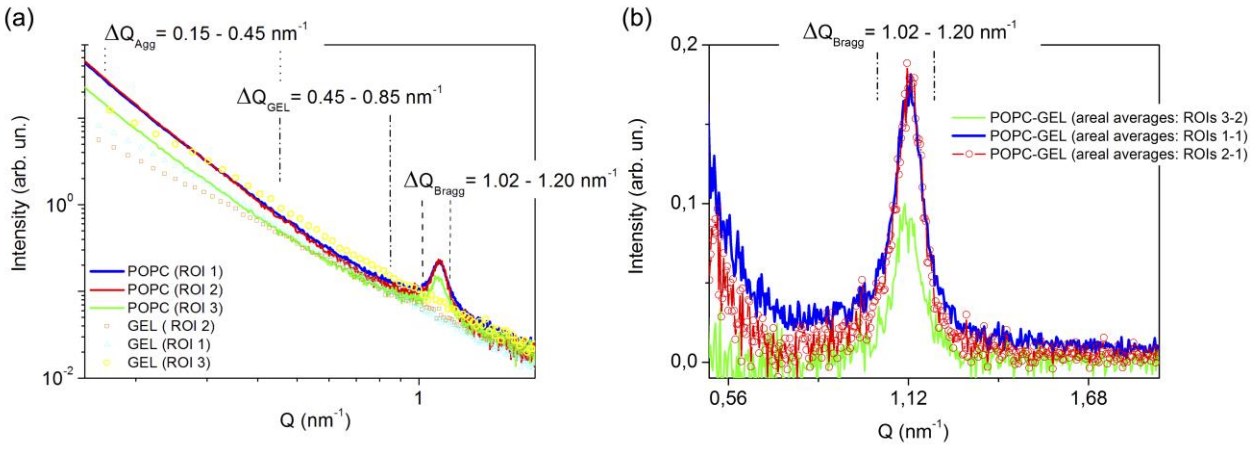


**Fig. S7. (**a) 1D-folded SAXS profiles (areal averages) from the ROIs selected in the POPC and GEL dry samples (Fig. 2 of the main text). (b) difference profiles obtained from the plots in (a), by subtracting the profile from ROI 1/2 in the GEL sample as a buffer for the profiles from ROIs 1,2/3 in the POPC sample, respectively. The selected GEL profiles thus account for the baseline under the Bragg peak.

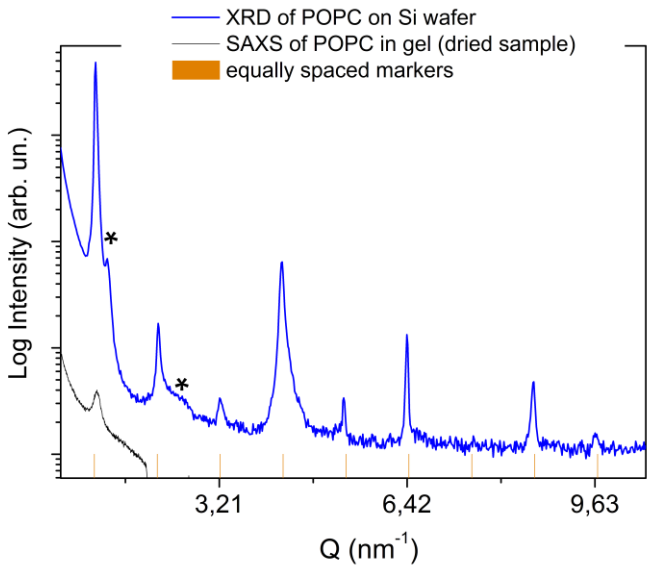


**Fig. S8.** XRD sample-detector scan ($\theta/2\theta$) of POPC layers directly deposited on a Si wafer (blue line) is compared with a typical 1D-folded SAXS pattern from the microscopy in Fig. 2g of the main text. Orange equally spaced markers indicate the main periodicity of the stacked lipids ($5.90 \pm 0.06$ nm); asterisks indicate a further minority periodicity.

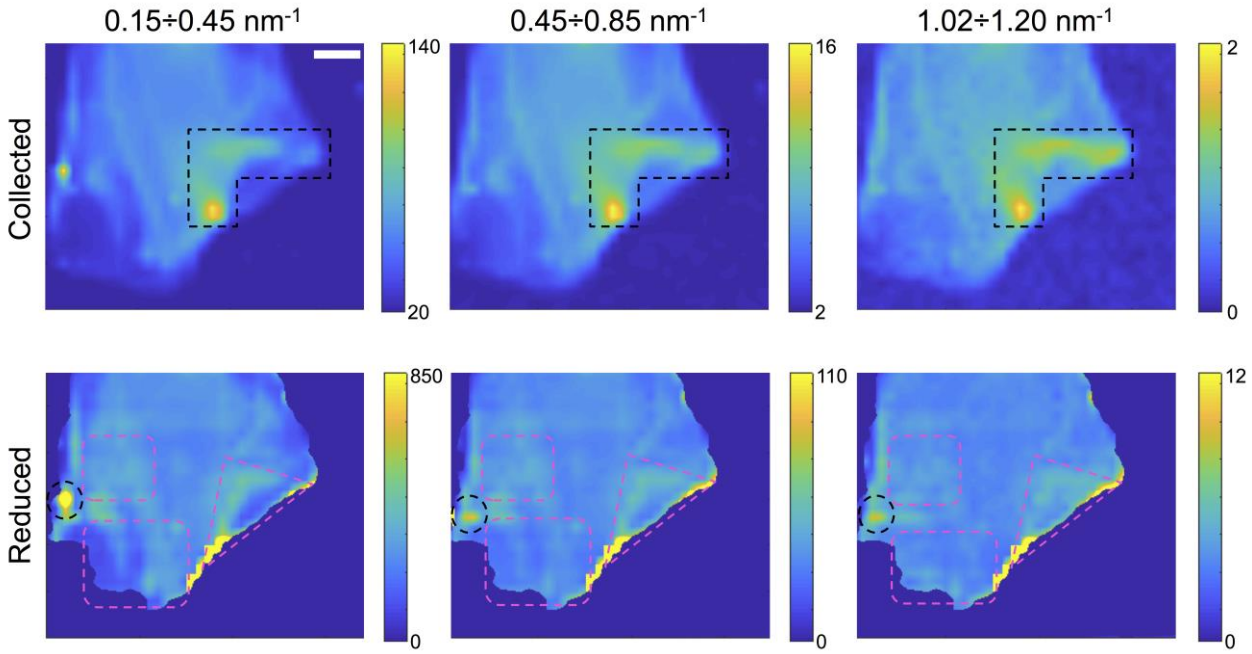


**Fig. S9.** SAXS maps in different Q-ranges for the dried GEL sample. From left to right (in both rows): 0.15÷0.45, 0.45÷0.85 , 1.02÷1.20 $nm^{-1}$. Upper row: as collected data; lower row: reduced data. Upper row: the black box indicates high density regions showing up in the as-collected microscopies. Lower row: magenta boxes indicate tiny differences in the scattering intensity as a function of the Q-range; the black circle indicates a bright spot ascribed to a big aggregate which produces high SAXS intensity only at low Q values. The saturated yellow regions at the right borders are due to vanishing sample thickness.

**References**

[1] Juan M. Montes De Oca-Ávalos; Davide Altamura; Maria Lidia Herrera; Cristián Huck-Iriart; Francesco Scattarella; Dritan Siliqi; Cinzia Giannini; Roberto Jorge Candal. Physical and structural properties of whey protein concentrate - corn oil - TiO2 nanocomposite films for edible food-packaging. Food Packaging and Shelf Life, 26 (2020).

[2] Mildner, Hall. Small-angle scattering from porous solids with fractal geometry. J Phys D. Appl Phys (1986), 9, 1535-1545.

[3] B Cabane, *Small Angle Scattering Methods*, in *Surfactant Solutions: New Methods of Investigation*, Ch.2, Surfactant Science Series Vol. 22, Ed. R Zana and M Dekker, New York, (1987).

[4] Guinier, A., Fournet, G. & Walker, C. (1955). Small Angle Scattering of X-rays. New York: J. Wiley & Sons.